



A Study on New Straight Shape Design to Reduce Cogging Torque of Small Wind Power Generator

Junho Kang ¹, Ju Lee ¹, Sanghwan Ham ², Yondo Chun ³  and Hyunwoo Kim ^{1,*} 

¹ Department of Electrical Engineering, Hanyang University, Seoul 04763, Republic of Korea; rwg1783@hanyang.ac.kr (J.K.); julee@hanyang.ac.kr (J.L.)

² Department of Electrical and Railway Engineering, Kyungil University, Gyeongsan-si 38428, Republic of Korea; shham@kiu.kr

³ Electric Machine and Drive Research Center, Korea Electrotechnology Research Institute, Changwon 51543, Republic of Korea; ydchun@keri.re.kr

* Correspondence: khw7481@hanyang.ac.kr

Abstract: In this paper, a 150 W small wind power generator which has a permanent magnet synchronous generator type is proposed with a new straight shape stator and rotor to reduce the cogging torque. The advantages of the proposed structure are introduced through a comparison between the basic and the proposed models. By comparing the pole slot combination of the proposed generator, the combination with optimal cogging torque characteristics was selected. The electromagnetic characteristics of the proposed shape are analyzed for design variables using a finite element analysis of ANSYS 2021 R1 Maxwell. The final model of the proposed structure is designed by considering the cogging torque and electromagnetic characteristics of the generator. The electromagnetic and structural simulations of the final model are performed to satisfy the required performance of the generator and mechanical safety. To verify the FEA results of the final model, a prototype is manufactured, experimented, and compared with the FEA results.

Keywords: cogging torque; electromotive force; permanent magnet synchronous generator; total harmonic distortion; wind power generator



Citation: Kang, J.; Lee, J.; Ham, S.; Chun, Y.; Kim, H. A Study on New Straight Shape Design to Reduce Cogging Torque of Small Wind Power Generator. *Machines* **2024**, *12*, 412. <https://doi.org/10.3390/machines12060412>

Academic Editor: Parviz Famouri

Received: 26 April 2024

Revised: 5 June 2024

Accepted: 14 June 2024

Published: 15 June 2024



Copyright: © 2024 by the authors. Licensee MDPI, Basel, Switzerland. This article is an open access article distributed under the terms and conditions of the Creative Commons Attribution (CC BY) license (<https://creativecommons.org/licenses/by/4.0/>).

1. Introduction

Recently, problems such as fossil fuel depletion, environmental pollution, and global warming issues are becoming more serious every year. Interest in producing electricity from renewable resources and cases of its application are increasing [1,2]. Representative renewable resources include solar power and wind power. Wind power generation has the advantage of being environmentally friendly, low production costs, and an infinite resource. Compared to solar power generation, wind power generation has the advantage of lower unit installation costs and lower production costs per unit for the same capacity [3,4]. Wind power generation systems are applied in a variety of ways, from large-scale power generation in offshore areas and small-scale in portable machines [5–7].

Generators using PM (permanent magnet) are widely used for wind power generators due to their advantages such as high energy density, high efficiency, and small size [7–9]. Small-scale PM generators have a simple structure and are often designed with a strong internal rotor. Generators require a tooth and slot structure to wind the coils on the stator. Due to the tooth structure, a spatial permeance difference occurs, which causes cogging torque. Since wind power exceeding cogging torque is required for the generator to operate, cogging torque reduction is necessary for the generator to operate in light winds [10,11].

Various studies are being conducted to reduce the cogging torque of wind power generators [12–14]. Since cogging torque is inversely proportional to the size of the LCM (least common multiple) of the number of poles and the number of slots, the cogging torque can be reduced by applying fractional slot concentrated winding (FSCW) with the

number of slots per pole being one or less [15,16]. The cogging torque can be reduced by adjusting the spatial permeance difference through stator and rotor skew, the pole arc ratio of PMs, and tapering [17–22]. Research is also being conducted to reduce cogging torque by optimizing the length of the slot opening, which is the main cause of spatial permeability differences, or by adding magnetic wedges [23,24]. To reduce the cogging torque, the LCM is mainly changed by selecting the pole slot combination, or the generator shape design variables are optimized to reduce the spatial permeance difference.

In this paper, a new generator structure for reducing cogging torque is introduced. The advantages of the proposed structure are discussed by a comparison with the basic model which has the arc shape of the stator and permanent magnet. By comparing the pole slot combinations for the proposed structure, the number of poles and slots with small cogging torque and high EMF (electromotive force) characteristics is selected. Using ANSYS 2021 R1 Maxwell, FEA for the electromagnetic design of the proposed model is conducted and the final shape of the proposed model is designed. The electromagnetic and structural simulation results of the final model are shown, and a comparison between the basic and final models is conducted. The final model of the proposed generator was manufactured, and the comparison with FEA and experiment results was performed to verify the FEA.

This paper is organized as follows. In Section 2, the definition and equation of cogging torque are introduced, and it is discussed how to reduce cogging torque through equations. In Section 3, the specifications and proposed shape for the small wind generator are introduced. In Section 4, the design method of the proposed model is discussed, and a comparison with the FEA results and experiment results of the prototype is conducted to verify the final model. Finally, Section 5 presents the conclusion.

2. Definition and Equation of Cogging Torque

Cogging torque is energy variation according to magnet angular position. Because the energy change in the PM and core is negligible than the airgap, the magnetostatic energy can be written as shown in Equation (1) [25]:

$$\begin{aligned} W(\alpha) \approx W(\alpha)_{airgap} &= \frac{1}{2\mu_0} \int_V P^2(\theta) F_m^2(\theta, \alpha) dV \\ &= \frac{L_{stk}}{4\mu_0} (R_2^2 - R_1^2) \int_0^{2\pi} G^2(\theta) B^2(\theta, \alpha) d\theta \end{aligned} \quad (1)$$

where μ_0 is the permeability of air, θ is the rotational angle, $P(\theta)$ is the airgap permeance function, $F_m(\theta, \alpha)$ is the airgap MMF (magnetomotive force) function, α is the rotational angle of rotor, L_{stk} is the stack length, R_1 and R_2 is PM and stator radius, $G(\theta)$ is the relative airgap permeance function, and $B(\theta)$ is the flux density function. Through Equation (1), the cogging torque can be derived from Equation (2):

$$T(\alpha) = \frac{\pi L_{stk}}{4\mu_0} (R_2^2 - R_1^2) \sum_0^{\infty} n N_L G_{nN_L} B_{nN_L} \sin n N_L \alpha \quad (2)$$

where n is the harmonic order, N_L is the LCM of the number of poles and slots, G_{nN_L} and B_{nN_L} are the design coefficients of stator teeth and PM. As shown in Equation (2), to reduce cogging torque, it is necessary to reduce G_{nN_L} by changing the stator shape, such as teeth notching or asymmetric shoe, or B_{nN_L} by changing the rotor shape, such as PM shaping or adjusting the pole arc ratio. However, this method can significantly reduce EMF, output, and efficiency. In this paper, a new stator and rotor structure is proposed that significantly reduces cogging and does not reduce EMF significantly compared to basic structures.

3. Specifications and Shape of Proposed Generator

In this section, the specifications of the target generator are introduced. The structures of the basic and proposed models are compared. The electromagnetic field characteristics

of the basic and proposed models are confirmed and the advantages of the proposed model over the basic model are shown.

3.1. Specifications of Generator

Small wind power generators require not only high efficiency and low THD (total harmonic distortion) because it may be linked to the prevailing power source, but also low cogging torque for starting in light winds. Table 1 shows the required specifications of the target small wind power generator.

Table 1. Specifications of target generator.

Parameter	Value	Unit
Power	150	W
Voltage	20	V
Base Speed	2000	RPM
Cogging Torque	15	mNm _{pk-pk}
THD of EMF (Line-Line)	5	%

3.2. Comparison of Base and Proposed Models

As can be seen in Equation (2), the cogging torque can be reduced by reducing G and B by applying a new structure. The structure proposed in this paper has a straight shape and has effects such as tapering and pole arc ratio. Figure 1a,b show the basic and proposed model of a small wind power generator. For comparison, the total usage of PMs for both models is the same. The basic model, as shown in Figure 1a, has a ring type PM.

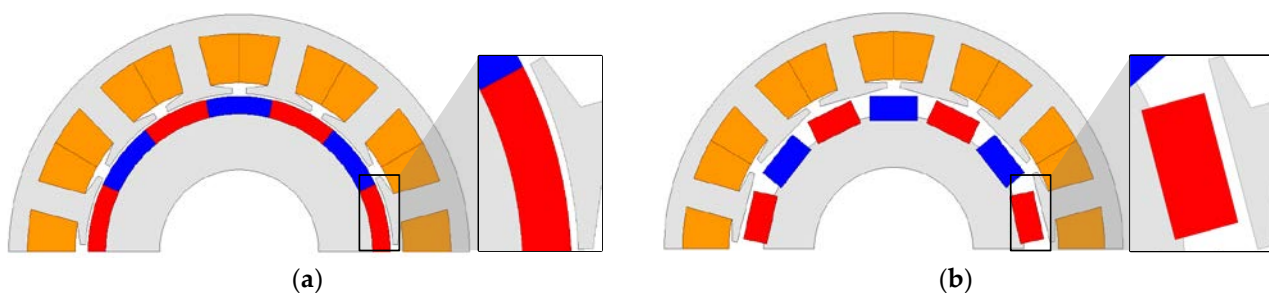


Figure 1. Shape of wind power generators (a) basic model (b) proposed model.

It has a circular shoe shape to maintain a constant airgap length, but the permeance decreases sharply at the slot opening between the stator teeth which causes cogging torque.

Considering the sudden change in spatial permeance, the proposed model as shown in Figure 1b selected the PM as a straight shape. The shoe of the teeth was also changed to have a constant airgap length according to the shape of the PM. Due to these changes in the rotor and stator shapes, the two coefficients in Equation (2) change. Figure 2 shows the waveforms of the airgap flux density and cogging torque of the two models. As can be seen in Figure 2a, the proposed model does not have large changes in airgap flux and has smaller cogging torque characteristics than the basic model, as shown in Figure 2b.

Since the permeance of the proposed structure according to position appears sinusoidally compared to the basic model which has large permeance changes between teeth, the proposed structure has small values of $G_{a_{nNL}}$ and $B_{a_{nNL}}$. As can be seen in Equation (2), the cogging torque of the proposed structure is smaller than that of the basic model for the same size.

Figure 3 shows the EMF waveform and FFT (fast Fourier transform) results of the two models. The basic model is superior in terms of EMF and THD characteristics.

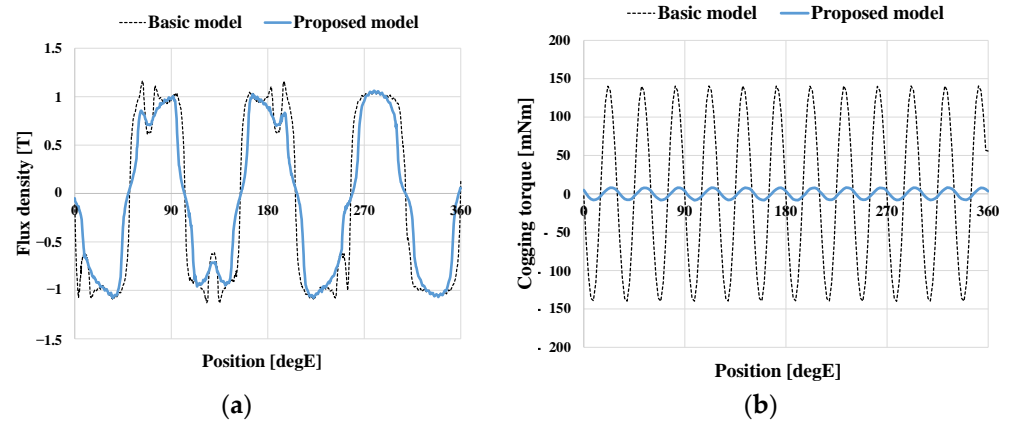


Figure 2. Characteristics of two models (a) airgap magnetic flux density (b) cogging torque.

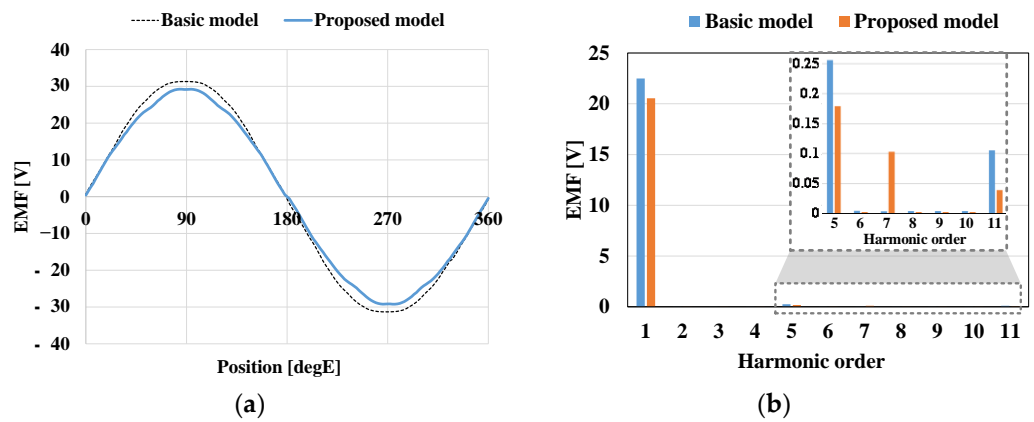


Figure 3. EMF characteristics of two models (a) waveform (b) FFT.

Figure 4 shows the flux lines of the basic and proposed models. The basic model has a large leakage flux between PMs, but the proposed model has a smaller leakage flux than the basic model due to the gap between PMs.

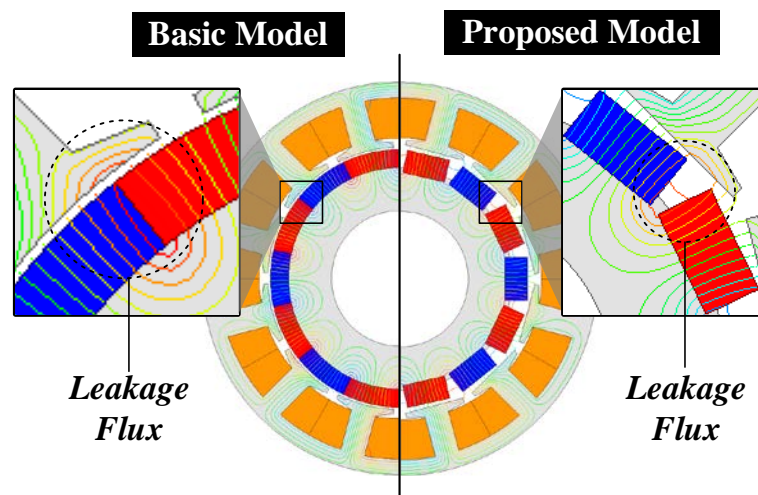


Figure 4. Flux lines of the basic and proposed models.

As shown in Figure 3a,b, the EMF appears high because the length of the air gap is constant and small, but in the proposed model, the air gap length varies depending on the angular position and the average air gap length is larger than the basic model.

Table 2 shows the characteristics of the basic and proposed models. When the power is the same, the efficiency of the proposed model is 0.2%p less than the basic model. However, the THD of the two models is the same, and the cogging torque of the proposed model is significantly reduced compared to the basic model. In this paper, the proposed model was selected to reduce the cogging torque, and an additional design was conducted to improve the efficiency and THD.

Table 2. Characteristics of the basic and proposed models.

Parameter	Basic Model	Proposed Model	Unit
Power	156.8	157.2	W
Efficiency	91.2	90.9	%
EMF	22.5	20.5	V_{rms}
THD of EMF (Line-Line)	1.3	1.3	%
Cogging Torque	280.7	16.2	mNm_{pk-pk}

4. Electromagnetic Design of Proposed Wind Generator

In this section, tendencies according to the design variables of the proposed structure are analyzed using FEA through ANSYS 2021 R1 Maxwell, and the final model is derived. The characteristics of the proposed structure according to the pole slot combination are compared. Design variables that can be selected in the proposed structure are introduced, each tendency is analyzed through FEA, and design points are determined to derive the final model.

4.1. Pole Slot Combinations

Wind power generators generally adopt a fractional slot concentrated winding (FSCW), where the number of slots per pole per phase is less than 1 for small cogging torque and high power density. Table 3 shows the winding factor according to the pole slot combination. The pole slot combination with a high winding coefficient must be selected to achieve high power density. As shown in Equation (2), the other factor is the LCM of the number of poles and slots. The higher number of the LCM, the smaller the cogging torque appears [26]. In this paper, generally used representative pole slot combinations (10P12S, 14P12S, 14P18S, and 16P18S) were selected, and the corresponding EMF, THD, and cogging torque characteristics were confirmed. For equal comparison, the amount of PMs used and the equivalent number of turns for each model were selected to be the same. Figure 5 shows the characteristics according to the pole slot combination. Figure 5 shows that the 14P12S model has a high EMF, low THD, and cogging torque. In this paper, the 14P12S combination was selected, and shape variable design was performed.

Table 3. Winding factor according to pole slot combination.

$N_{slot} \setminus N_{pole}$	4	6	8	10	12	14	16
6	0.866	-	0.866	0.5	-	0.5	0.866
9	0.617	0.866	0.945	0.945	0.866	0.617	0.328
12	-	-	0.866	0.933	-	0.933	0.866
15	-	-	0.621	0.866	-	0.951	0.951
18	-	-	-	0.647	0.866	0.902	0.945

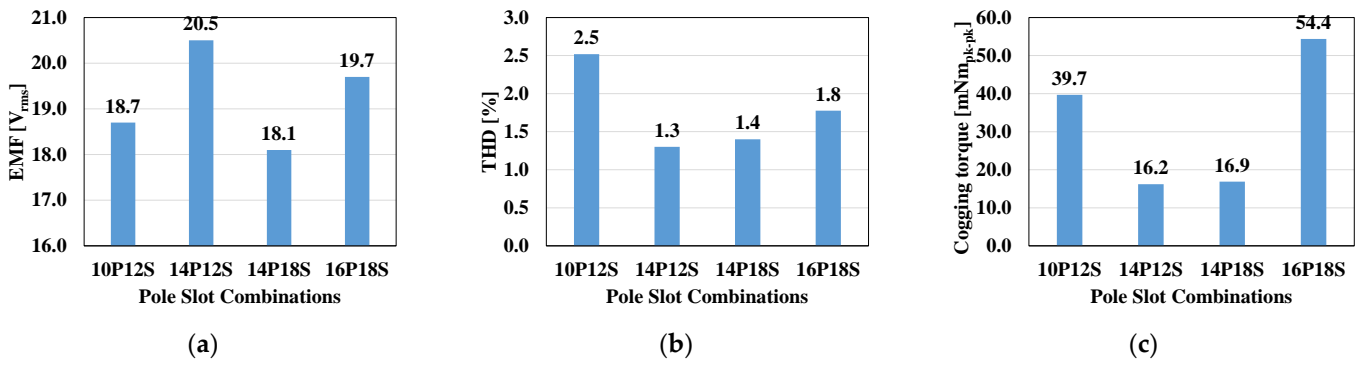


Figure 5. Characteristics according to pole slot combination: (a) EMF; (b) THD; (c) cogging torque.

4.2. Airgap

Figure 6 shows the design variables of the proposed model. In the proposed model, the PM has a straight shape, so the maximum rotor radius is from the origin to the PM vertex. Therefore, as shown in Figure 6, the minimum airgap length (g_{\min}) from the PM vertex to the center of the shoe is selected.

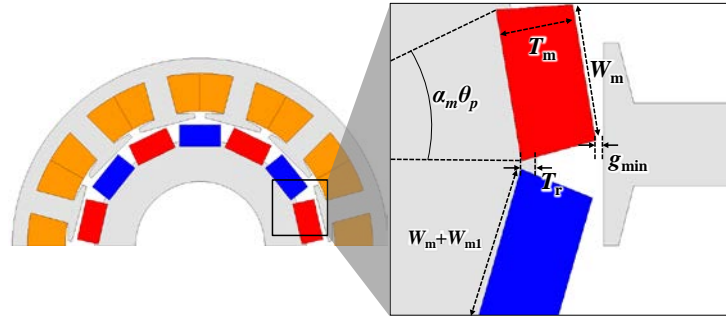


Figure 6. Design variables of the proposed model.

4.3. Magnet

When the rotor outer diameter is fixed, the maximum PM width is determined by the PM thickness. Equations (3) and (4) represent the PM width according to the rotor outer diameter and PM thickness, and is the maximum PM width that can be selected when the pole arc ratio is 1:

$$W_m = \left(\frac{2k}{1+k^2} \right) \left(\sqrt{T_m^2 - (1+k^2) \left(T_m^2 - \frac{D_{ro}^2}{4} \right)} - T_m \right) \quad (3)$$

$$k = \tan \left(\alpha_m \frac{180 \text{deg}}{N_{pole}} \right) \quad (4)$$

where W_m is the PM width, T_m is the PM thickness, D_{ro} is the rotor outer diameter, α_m is the pole arc ratio, and N_{pole} is the number of poles. As the PM thickness increases, the maximum width that can be selected decreases.

As shown in Equation (3), T_m and W_m are inversely proportional. Because the length of the permanent magnet occupied by one pole varies depending on T_m , characteristics such as cogging torque change. Figure 7 shows the characteristics of the proposed model according to PM thickness. Design is required at a point where the cogging torque is minimum, the target EMF is satisfied, and the THD is small. When inserting the PM of the proposed model into the rotor, if the PM has a rectangular shape, it may scatter when the generator is driven. Therefore, a structure is adopted in which the rotor core can support the PM through a small additional length (W_{m1}) of about 0.2 mm of the inner side of the PM.

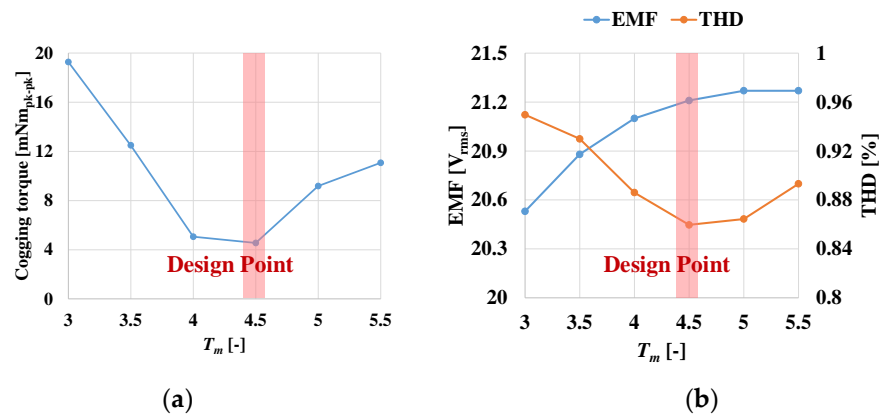


Figure 7. Characteristics according to T_m (a) cogging torque (b) EMF and THD.

As shown in Equations (3) and (4), the shape of the permanent magnet changes depending on the pole arc ratio, affecting the electromagnetic field characteristics. Figure 8 shows the characteristics of the proposed model according to the pole arc ratio. As the pole arc ratio increases, the use of PMs and EMF increases. Moreover, there is an optimal point for THD and cogging torque. The optimal design point is selected by considering the cogging torque, EMF characteristics, the usage of the PM of the basic model, and constraints as shown in Figure 8.

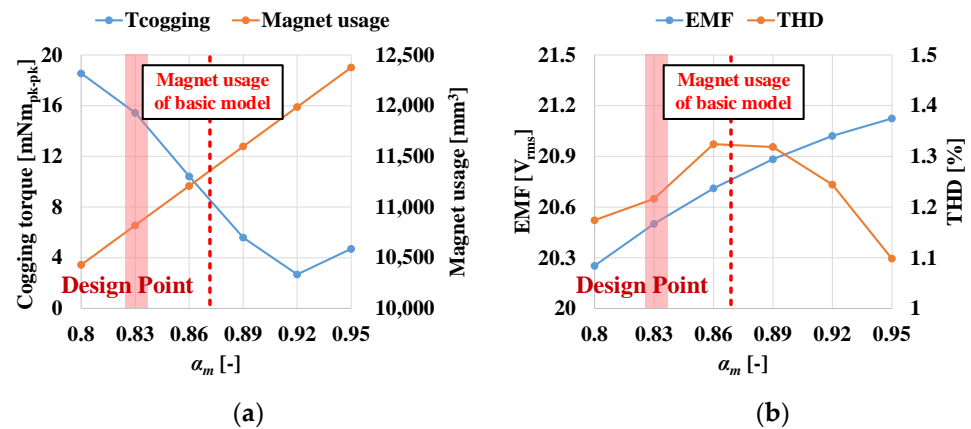


Figure 8. Characteristics according to α_m (a) cogging torque and magnet usage (b) EMF and THD.

4.4. Rotor Core

Figure 9 shows the flux line according to the magnet insertion depth. In Figure 9a, because of lack of iron between the PMs, the leakage flux between the PMs flows through the air. In Figure 9b, because of the core between the PMs, the leakage flux flows through iron. As can be seen in Figure 9, when a PM is inserted into the rotor core, the electromagnetic characteristics may vary depending on the insertion depth because of leakage flux between the PMs. Because the average air gap length and leakage flux change depending on the PM insertion depth, there is an optimal point for cogging torque and EMF.

Figure 10 shows the cogging torque and EMF characteristics according to the PM insertion depth (T_r). Because the average air gap length and leakage flux change depending on the PM insertion depth, there is an optimal point for cogging torque and EMF, as shown in Figure 10. Considering design constraints, a point was selected that maximizes EMF and has low cogging torque for high efficiency.

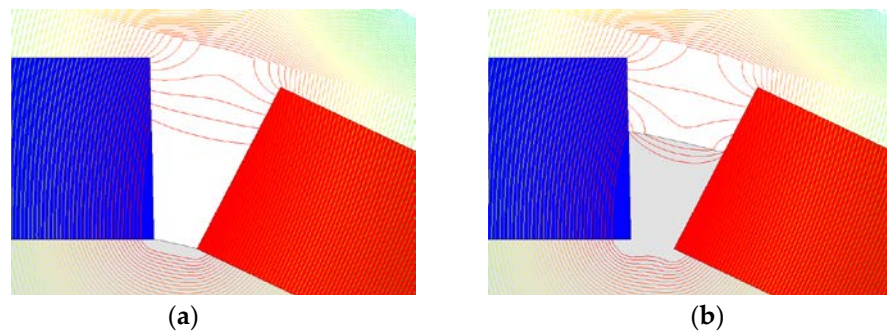


Figure 9. Flux line according to T_r : (a) $T_r = 0$ mm (b) $T_r = 3$ mm.

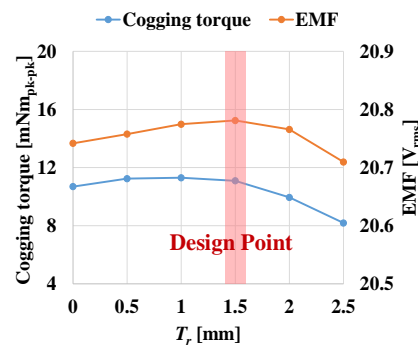


Figure 10. Characteristics according to T_r .

4.5. FEA Results of Final Model

The design of the final model is carried out based on the design variable analysis conducted in the previous chapters. Table 4 shows the value of design variables for the final model. Figure 11a shows the final shape of the proposed model, Figure 11b shows the mesh plot for FEA analysis, and Figure 11c shows the magnetic flux density distribution.

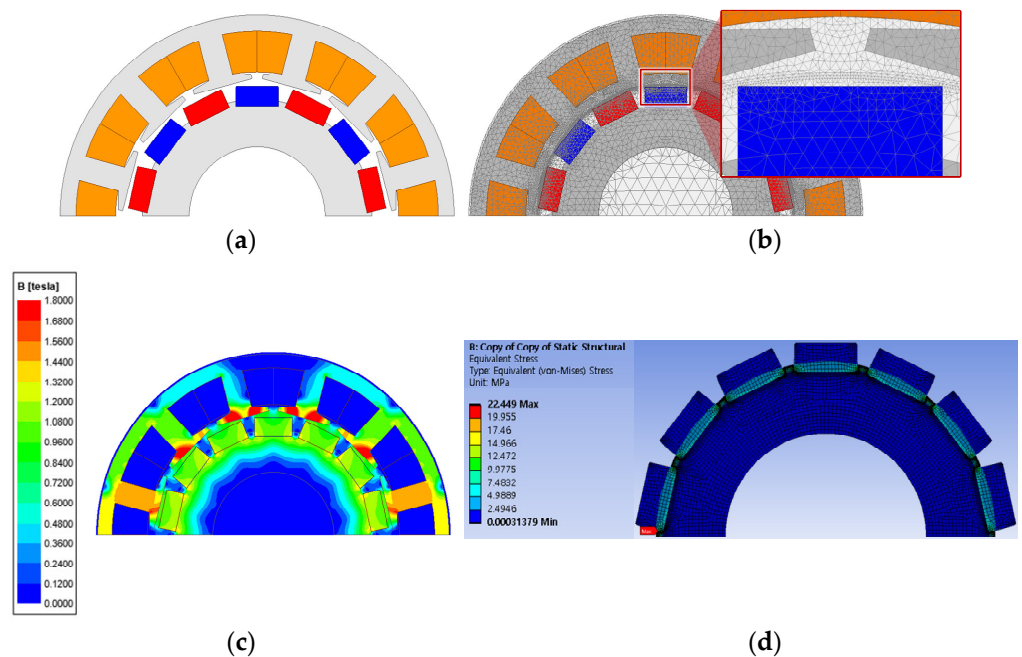


Figure 11. Final model (a) FEA model (b) mesh plot (c) magnetic flux density distribution (d) result of structural simulation.

Table 4. Value of design variables.

Variable	Value	Unit
PM Thickness (T_m)	4.5	mm
PM Width (W_m)	8.9	mm
Additional Inner PM Width (W_{m1})	0.2	mm
Pole Arc Ratio (α_m)	0.83	mm
PM Insertion Depth (T_r)	1.5	mm

Since PMs may scatter due to stress when driving a generator, it is necessary to analyze the stress. Figure 11d is the structural simulation result of the proposed model rotor. In general, the safety factor is the index of the mechanical reliability and is calculated as Equation (5) [27]:

$$\text{Safety Factor} = \frac{\text{Yield Stress}}{\text{Maximum Working Stress}} \quad (5)$$

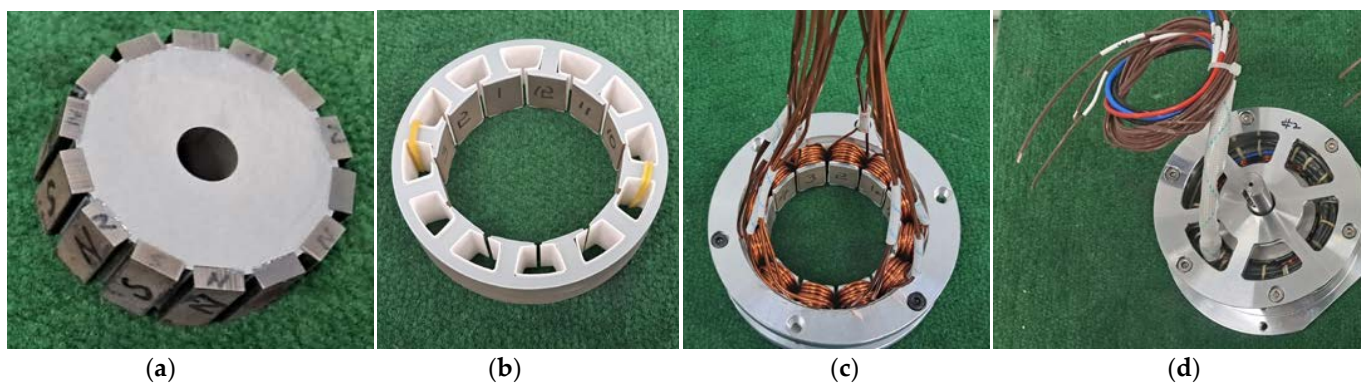
In general, the generator is safe from stress if the safety factor exceeds 2. The safety factor of the final model is about 19.6, which confirms that it is safe from stress. Table 5 shows the design results of the basic and final model. The size and output power of the two models are the same. In the final model, THD increased by 0.1%p and the efficiency decreased by 0.2%p, but cogging torque was significantly reduced by 96% compared to the basic model.

Table 5. Design results of the basic and final models.

Parameter	Basic Model	Final Model	Unit
Stator Outer Diameter	87	87	mm
Stack Length	20	20	mm
Power	156.8	156.8	W
Voltage	20.5	20.1	V _{rms}
Base Speed	2000	2000	RPM
Cogging Torque	280.7	11.7	mNm _{pk-pk}
THD	1.3	1.4	%
Copper Loss	4.5	5.6	W
Core Loss	7.1	6.6	W
Magnet Loss	0.7	0.4	W
Efficiency	91.2	91.0	%

4.6. Manufacture and Experiment Verification

To verify the FEA results, the prototype of the final model was manufactured. Figure 12 shows the manufactured prototype.

**Figure 12.** Prototype of the final model: (a) rotor; (b) stator; (c) coil in stator; and (d) assembled wind power generator.

No-load experiments were conducted on the prototype at 1600 RPM. Figure 13a,b show the prototype's EMF waveform of the no-load and load FEA results, and Figure 13c shows the EMF waveform of no-load. The FEA and experiment of EMF were 8.21 V and 8.03 V, respectively. Load experiments were conducted on the prototype at 2000 RPM. The value of the load resistance was adjusted so that the power of the generator was more than 150 W. The output, terminal voltage, and efficiency were measured by load experiments. Table 6 shows that the FEA and experiment results of the wind power generator. For the same power, the terminal voltage and efficiency errors of both models are less than 1%.

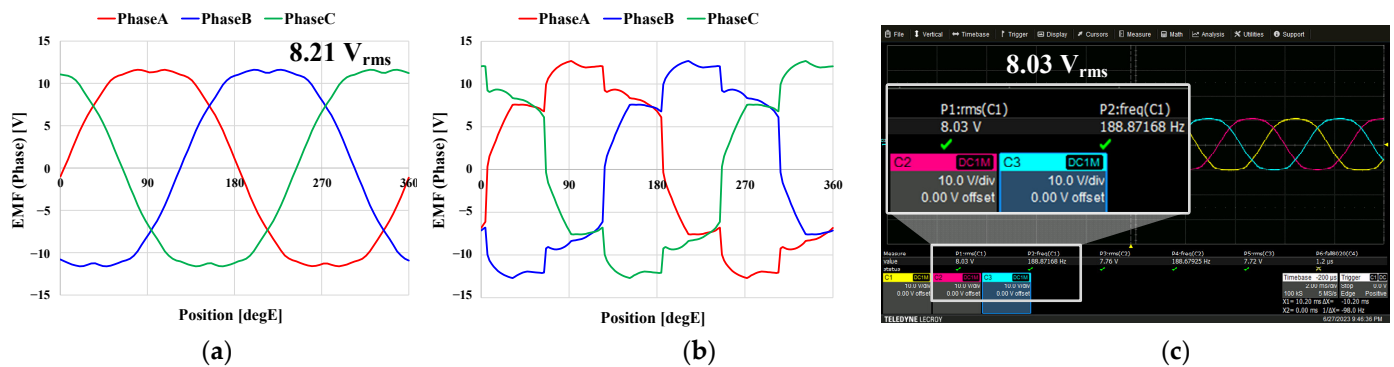


Figure 13. EMF waveform (1600 RPM): (a) FEA (no-load); (b) FEA (load); and (c) experiment (no-load).

Table 6. FEA and experiment results of the wind power generator.

Parameter	FEA	Experiment	Unit
Power	156.8	160.4	W
EMF (@1600 RPM)	8.21	8.03	V _{rms}
Voltage	20.1	20.0	V
Efficiency	91.0	90.8	%

5. Conclusions

In this paper, a small wind turbine structure with a straight shape to reduce the cogging torque is proposed. The proposed model is compared to a basic model with ring type and its advantages are shown. The final model is derived by selecting and analyzing variables for the design of the proposed structure. The final model is compared to the basic model and shows a significant reduction in cogging torque. A prototype has been created, and the validation of the study is verified through comparison with the experiment and FEA results.

Author Contributions: Conceptualization, J.K. and H.K.; methodology, J.K.; validation, J.K.; investigation, J.K. and S.H.; writing—original draft preparation, J.K.; writing—review and editing, Y.C. and J.L.; visualization, J.K.; supervision, H.K. and J.L.; project administration, J.K. and S.H.; funding acquisition, Y.C. and J.L. All authors have read and agreed to the published version of the manuscript.

Funding: This research was supported by Korea Electric Power Corporation. (Grant number: R22XO02-02) and in part by the Nano & Material Technology Development Program through the National Research Foundation of Korea (NRF) funded by Ministry of Science and ICT (No. 2020M3H4A3106178).

Data Availability Statement: The data presented in this study are available in this article.

Conflicts of Interest: The authors declare no conflicts of interest.

References

- Seangwong, P.; Chamchuen, S.; Fernando, N.; Siritaratiwat, A.; Khunkitti, P. A Novel Six-Phase V-Shaped Flux-Switching Permanent Magnet Generator for Wind Power Generation. *Energies* **2022**, *15*, 9608. [[CrossRef](#)]

2. Seangwong, P.; Fernando, N.; Siritaratiwat, A.; Khunkitti, P. E-Core and C-Core Switched Flux Permanent Magnet Generators for Wind Power Generation. *IEEE Access* **2023**, *11*, 138590–138601. [[CrossRef](#)]
3. Lee, S.-H.; Kim, Y.-J.; Lee, K.-S.; Kim, S.-J. Multiobjective Optimization Design of Small-Scale Wind Power Generator with Outer Rotor Based on Box–Behnken Design. *IEEE Trans. Appl. Supercond.* **2016**, *26*, 1–5. [[CrossRef](#)]
4. Mahdavi, M.; Jurado, F.; Schmitt, K.; Chamana, M. Electricity Generation from Cow Manure Compared to Wind and Photovoltaic Electric Power Considering Load Uncertainty and Renewable Generation Variability. *IEEE Trans. Ind. Appl.* **2024**, *60*, 3543–3553. [[CrossRef](#)]
5. Manne, B.; Kumar, M.K.; Akuru, U.B. Design and Performance Assessment of a Small-Scale Ferrite-PM Flux Reversal Wind Generator. *Energies* **2020**, *13*, 5565. [[CrossRef](#)]
6. Li, J.; Yang, G.; Rao, F. Analysis and Design of Novel Axial Field Flux-Modulation Permanent Magnet Machines for Direct Drive Application. *Machines* **2022**, *10*, 495. [[CrossRef](#)]
7. Lee, J.-Y.; Koo, D.-H.; Moon, S.-R.; Han, C.-K. Design of an Axial Flux Permanent Magnet Generator for a Portable Hand Crank Generating System. *IEEE Trans. Magn.* **2012**, *48*, 2977–2980. [[CrossRef](#)]
8. Jang, S.-M.; Park, H.-J.; Choi, J.-H.; Han, C.; Choi, M.-S. Analysis on the Magnetic Force Characteristics of Segmented Magnet Used in Large Permanent-Magnet Wind Power Generator. *IEEE Trans. Magn.* **2013**, *49*, 3981–3984. [[CrossRef](#)]
9. Zhu, G. Design Optimization of a HTS-Modulated PM Wind Generator. *IEEE Trans. Appl. Supercond.* **2021**, *31*, 1–4. [[CrossRef](#)]
10. García-Gracia, M.; Jiménez Romero, Á.; Herrero Ciudad, J.; Martín Arroyo, S. Cogging Torque Reduction Based on a New Pre-Slot Technique for a Small Wind Generator. *Energies* **2018**, *11*, 3219. [[CrossRef](#)]
11. Hsieh, M.-F.; Yeh, Y.-H. Rotor Eccentricity Effect on Cogging Torque of PM Generators for Small Wind Turbines. *IEEE Trans. Magn.* **2013**, *49*, 1897–1900. [[CrossRef](#)]
12. Kim, D.-H.; Kim, K.-S.; Yang, I.-J.; Lee, J.; Kim, W.-H. Alternative Bridge Spoke Permanent Magnet Synchronous Generator Design for Wind Power Generation Systems. *IEEE Access* **2021**, *9*, 152819–152828. [[CrossRef](#)]
13. Kim, D.-H.; Pyo, H.-J.; Kim, W.-H.; Lee, J.; Lee, K.-D. Design of Spoke-Type Permanent Magnet Synchronous Generator for Low Capacity Wind Turbine Considering Magnetization and Cogging Torques. *Machines* **2023**, *11*, 301. [[CrossRef](#)]
14. Sun, Y.; Bianchi, N.; Ji, J.; Zhao, W. Improving Torque Analysis and Design Using the Air-Gap Field Modulation Principle for Permanent-Magnet Hub Machines. *Energies* **2023**, *16*, 6214. [[CrossRef](#)]
15. Abdel-Khalik, A.S.; Ahmed, S.; Massoud, A.M.; Elserougi, A.A. An Improved Performance Direct-Drive Permanent Magnet Wind Generator Using a Novel Single-Layer Winding Layout. *IEEE Trans. Magn.* **2013**, *49*, 5124–5134. [[CrossRef](#)]
16. Du, Y. Investigation of Post-Demagnetization Torque Ripple in Fractional-Slot Surface-Mounted PM Wind Power Generators After Short Circuit Faults. *IEEE Ind. Appl.* **2024**, *60*, 215–228. [[CrossRef](#)]
17. Jang, S.-M.; Seo, H.-J.; Park, Y.-S.; Park, H.-I.; Choi, J.-Y. Design and Electromagnetic Field Characteristic Analysis of 1.5 kW Small Scale Wind Power Generator for Substitution of Nd-Fe-B to Ferrite Permanent Magnet. *IEEE Trans. Magn.* **2012**, *48*, 2933–2936. [[CrossRef](#)]
18. Goryca, Z.; Różowicz, S.; Różowicz, A.; Pakosz, A.; Leško, M.; Wachta, H. Impact of Selected Methods of Cogging Torque Reduction in Multipolar Permanent-Magnet Machines. *Energies* **2020**, *13*, 6108. [[CrossRef](#)]
19. Wang, Q.; Zhao, B.; Zou, J.; Li, Y. Minimization of Cogging Force in Fractional-Slot Permanent Magnet Linear Motors with Double-Layer Concentrated Windings. *Energies* **2016**, *9*, 918. [[CrossRef](#)]
20. Neto, M.G.; da Silva, F.F.; Branco, P.J.d.C. Operational Analysis of an Axial and Solid Double-Pole Configuration in a Permanent Magnet Flux-Switching Generator. *Energies* **2024**, *17*, 1698. [[CrossRef](#)]
21. Torn, V.; Seangwong, P.; Fernando, N.; Siritaratiwat, A.; Khunkitti, P. Performance Improvement of Flux Switching Permanent Magnet Wind Generator Using Magnetic Flux Barrier Design. *Sustainability* **2023**, *15*, 8867. [[CrossRef](#)]
22. Onsal, M.; Cumhur, B.; Demir, Y.; Yolacan, E.; Aydin, M. Rotor Design Optimization of a New Flux-Assisted Consequent Pole Spoke-Type Permanent Magnet Torque Motor for Low-Speed Applications. *IEEE Trans. Magn.* **2018**, *54*, 1–5. [[CrossRef](#)]
23. Zhao, X.; Jiang, J.; Niu, S.; Wang, Q. Slot-PM-Assisted Hybrid Reluctance Generator with Self-Excited DC Source for Stand-Alone Wind Power Generation. *IEEE Trans. Magn.* **2022**, *58*, 1–6. [[CrossRef](#)]
24. Liu, T.; Huang, S.; Gao, J.; Lu, K. Cogging Torque Reduction by Slot-Opening Shift for Permanent Magnet Machines. *IEEE Trans. Magn.* **2013**, *49*, 4028–4031. [[CrossRef](#)]
25. Hwang, S.-M. Cogging Torque and Acoustic Noise Reduction in Permanent Magnet Motors by Teeth Pairing. *IEEE Trans. Magn.* **2000**, *36*, 3144–3146. [[CrossRef](#)]
26. Cros, J.; Viarouge, P. Synthesis of high performance PM motors with concentrated windings. *IEEE Trans. Energy Convers.* **2022**, *17*, 248–253. [[CrossRef](#)]
27. Lee, J.-K. A Study on Analysis of Synchronous Reluctance Motor Considering Axial Flux Leakage Through End Plate. *IEEE Trans. Magn.* **2019**, *55*, 1–4. [[CrossRef](#)]

Disclaimer/Publisher’s Note: The statements, opinions and data contained in all publications are solely those of the individual author(s) and contributor(s) and not of MDPI and/or the editor(s). MDPI and/or the editor(s) disclaim responsibility for any injury to people or property resulting from any ideas, methods, instructions or products referred to in the content.